npj | Materials Degradation

www.nature.com/npjmatdeg

ARTICLE OPEN

Check for updates

High-temperature oxidation behaviour of Al_xFeCrCoNi and AlTiVCr compositionally complex alloys

Mohsen Esmaily[1,2]✉, Yao Qiu[2], Sedigheh Bigdeli[3], Mahesh B. Venkataraman[4], Antoine Allanore[1] and Nick Birbilis[4]

Compositionally complex alloys (CCAs), also termed as high entropy alloys (HEAs) or multi-principal element alloys (MPEAs), are being considered as a potential solution for many energy-related applications comprising extreme environments and temperatures. Herein, a review of the pertinent literature is performed in conjunction with original works characterising the oxidation behaviour of two diverse Al-containing alloys; namely a lightweight (5.06 g/cm^3) single-phase AlTiVCr CCA and a multiple-phase $Al_{0.9}$FeCrCoNi CCA (6.9 g/cm^3). The thermogravimetric results obtained during oxidation of the alloys at 700 and 900 °C revealed that both alloys tended to obey the desired parabolic rate law. Post-exposure analysis by means of electron microscopy indicated that while the oxide scale formed on the AlTiVCr is adherent to the substrate, the scale developed on the $Al_{0.9}$FeCrCoNi displays a notable spalling propensity. This study highlights the need for tailoring the protective properties of the oxide scale formed on the surface of the CCAs.

npj Materials Degradation (2020)4:25 ; https://doi.org/10.1038/s41529-020-00129-2

INTRODUCTION

High-temperature alloys and superalloys are essential for many critical applications involving corrosive chemical and electrochemical reactions including jet engines, land-based gas turbines, materials processing, as well as a wide range of emerging technologies such as concentrated solar thermal power (also known as concentrated solar plants (CSPs)), biomass gasification and molten oxide electrolysis (MOE)[1]. At elevated temperatures, alloys tend to react with the environment and form different "unwanted" products (e.g., oxides, nitrides, carbides, and sulphides), and if oxidation is unhindered, such reactions may wholly consume the alloy. As such, the ability of high-temperature alloys to form an adherent, slow-growing and protective surface oxide (scale), nominally consisting of chromia (Cr_2O_3) and alumina (Al_2O_3), is essential for sustained high temperature and harsh environment exposure without premature failure[1,2]. Of the two family of high-temperature materials, i.e., alumina-formers and chromia-formers, alloys forming protective Al_2O_3 scales such as iron (Fe)-based (FeCrAls)[1], nickel (Ni)-based (NiCrAls)[3], cobalt (Co)-based (CoCrAls)[4] and nickel aluminates (NiAl)-type materials[5] are considered for applications with operating temperatures >900 °C. This is because α-Al_2O_3 scale possess several characteristics that are highly desired for the high-temperature oxidation performance of alloys including: (i) they grow very slowly, (ii) thermodynamic stability, and (iii) chemically inert[1,2].

Despite sustained research and development in the field of high-temperature materials for many decades, there remains an ongoing desire for materials with improved high-temperature capabilities owing to demands for higher process efficiencies[1]. Presently, compositionally complex alloys (CCAs) are currently being considered as promising candidate materials for high-temperature applications owing to their high melting points, high-temperature strength (creep resistance), wear resistance and microstructural stability[6]. These alloys, by definition, consist of multiple elements in equimolar or near-equimolar ratios and tend to form metallic solid solutions (FCC, BCC, HCP, or a mixture of these)[6,7]. While CCAs exhibit sufficiently high melting points and phase stability for demanding applications, they, however remain dependent on the formation of a reliable protective oxide scale for continuity of usage, which is no different from "traditional" Fe-base and Ni-base alloys. At present, there is insufficient knowledge regarding the high-temperature oxidation behaviour of CCAs more generally, with relatively few studies reported such properties[8–22]. An overview of the limited research within the context of oxidation of CCAs at temperatures ranging from 500 to 1200 °C is provided in Table 1. Some of the findings of the previous publications (as reviewed in Table 1) are visually summarised in Fig. 1. It is noted that (i) the high-temperature oxidation of only a very limited number of CCAs have, to date, been studied, with the majority of studies focusing on either the CoCrFeNiX (X = Al, Mn, Si)[6,10,11] or MoCrTiAlY (Y = W, Nb, Ta)[14] systems, (ii) the two essential alloying elements, Cr[9] and Al[10], positively influence the oxidation properties of CCAs, and (iii) the surface oxide forming on CCAs containing Mn[10,16] and Cu[21] are prone to failure e.g. cracking and spallation, due to the formation of Mn-rich oxides. There have also been reports that reveal certain alloys, such as Al_xTiZrNbHfTa, are susceptible to "pesting", meaning that at high-temperatures they fully disintegrate into small pieces covered by loose voluminous oxides[22]. To further expand the current understanding on high-temperature oxidation behaviour of CCAs, in this study, the early stages of oxidation for AlTiVCr (5.06 g/cm^3) and $Al_{0.9}$FeCrCoNi (6.9 g/cm^3) were characterised using thermogravimetric analysis electron microscopy and thermodynamic calculations (by means of Thermo-Calc software) and the results were compared with those reported in the literature. Of the two CCAs, AlTiVCr is of interest for the energy-saving applications where high specific strength is required. In the context of high-temperature oxidation, to date, studies on Al_xFeCrCoNi-based CCAs are limited (see e.g., ref. [17]), and for the AlTiVCr CCA, no prior studies exist.

[1]Department of Materials Science and Engineering, Massachusetts Institute of Technology, Cambridge, MA 02139, USA. [2]Department of Materials Science and Engineering, Monash University, Melbourne, VIC 3800, Australia. [3]Department of Chemistry and Chemical Engineering, Chalmers University of Technology, 412 96 Gothenburg, Sweden. [4]College of Engineering and Computer Science, The Australian National University, Canberra, ACT 0200, Australia. ✉email: esmaily@mit.edu

Table 1. Summary of the previous research on high-temperature oxidation (corrosion) behaviour of HEAs.

Alloy	Exposure condition	Observation(s)	Ref.
$Al_xCoCrNi$(Fe or Si) -$Al_{0.44}CrCoNiFe$ -$Al_{0.8}CrCoNiSi$ *Effect of Al*	1050 °C Up to 200 h Furnace exposure	-Oxide (low Al content): External Cr_2O_3, internal Al_2O_3 and AlN; (high Al content): continuous and protective Al_2O_3 scale -Obeying parabolic growth law	Butler et al. (2015)[8]
CoCrFeMnNi CoNiFeMn *Effect of Cr*	650 and 750 °C 1100 h Furnace exposure	-Oxide: Cr_2O_3 with some Mn oxide (in the Cr-containing alloy) -Mn deteriorate the oxidation resistance -No internal oxidation	Holcomb et al. (2015)[9]
FeCoNiCrMn	PO_2 pressure from 10 to 105 Pa 950 °C	Oxide: An outer Mn_3O_4 layer, an intermediate $Mn_3O_4 + (Mn,Cr)_3O_4 + Cr_2O_3$, and an inner layer of Cr_2O_3. -Obeying parabolic growth law	Kai et al. (2016)[10]
CrMnFeCoNi	500–900 °C Up to 100 h TGA	-Oxide: Mn_2O_3 (with minor Cr_2O_3) at 600 & 700 °C; Mn_3O_4 at 900 °C -Internal oxidation -Linear and parabolic oxidation	Laplanche et al. (2016)[11]
$Cu_xAlCoCrFeNi$ ($x = 0, 0.5, 1$) *Effect of Cu*	1000 °C Up to 100 h TGA	-Oxide: α-Al_2O_3 -From protective scale to spallation by increasing the Cu content -Internal depletion of Al -Phase changes in the alloy	Dabrowa et al. (2017)[12]
FeCoNiCr-HEAs FeCoNiCrAl FeCoNiCrMn FeCoNiCrSi	Dry air 700–900 °C Up to 48 h TGA	-Oxide: metastable/stable forms of Al_2O_3 -Oxidation of Al-containing and Si-containing alloy was better than FeCoNiCr -Mn-containing alloy showed the worse oxidation performance -Obeying parabolic growth law	Kai et al. (2017)[13]
WMoCrTiAl NbMoCrTiAl TaMoCrTiAl and TaMoCrTiAl *micro-alloyed with Si*	900, 1000, and 1100 °C 50 h TGA	Oxide: Al-containing, Ti-containing, and Cr-rich oxides/layers -Inhomogeneous oxide scales -Ta-containing alloy showed the best oxidation performance, following the parabolic rate law for oxide growth -Extensive internal nitridation/oxidation -Si deteriorates the oxidation performance	Gorr et al. (2017)[14] Muller et al. (2018)[15]
CrMnFeCoNi	900, 1000, 1100 °C Up to 24 h TGA	-Oxides: Cr_2O_3 and Mn_2O_3 at 900 C; $(Mn.Cr)_2O_3$ and Mn_3O_4 at 1000 and 1100 °C -Internal oxidation and spallation of the scale at high temperatures	Kim et al. (2018)[16]
$Al_xTiZrNbHfTa$ ($x = 0–1$) *Effect of Al*	700, 1100 and 1300 °C 50 h Furnace exposure	-Oxide: Al-rich oxide scale -"Pesting" occurs at 700–900 °C in Al_0 alloy -Al improves the oxidation performance quite significantly -Poor oxidation resistance at 1300 °C -Mass gain twice of that of Ni-based alloys	Chang et al. (2018)[22]
$Al_xCoCrCuFeNi$ ($x = 0$, 0.5, 1, 1.5, 2) *Effect of Al*	1000 °C Up to 100 h Furnace exposure	-Oxide: Al_2O_3 (High Al content) and non-protective Cr_2O_3 (low Al) -Internal depletion of Al and Cr -Phase changes in the alloy	Liu et al. (2019)[18]
$CoCrFeNiAl_xT_{iy}$ ($x = 0.5$) CoCrFeNiAl0.5 CoCrFeNiAlTi0.5 *Effect of Al and Ti*	1000 °C Up to 100 h Furnace exposure	-Oxide: Al_2O_3 (Al containing) and mixed oxides (Ti containing alloy) -Positive effect of Al (the scale) -Ti worsen the oxidation resistance -Parabolic growth law (the Ti-lean alloy)	Erdogan et al. (2019)[19]
FeCoNiCrMn	CO_2/CO 700 and 950 °C 1100 h Furnace exposure	-Oxide: Mixture of MnO, $(Mn,Fe)_3O_4$, and $(Mn,Cr)_3O_4$ -No internal oxidation -Obeying parabolic growth law	Kai et al. (2019)[20]

Note that the oxidation exposures are in lab air unless otherwise specified.

RESULTS

Alloy microstructure

The microstructure of the AlTiVCr and $Al_{0.9}FeCrCoNi$ CCAs in the as-arc melted condition has been described in detail[23,24] (information on the alloy in "Methods" section). Shortly, the lightweight alloy (AlTiVCr) is single-phase CCA, displaying the characteristics of a uniform B2 structure (Fig. 2a), while the relatively high-density alloy ($Al_{0.9}FeCrCoNi$) is a multi-phase CCA, displaying FCC, BCC, and B2 phases (Fig. 2b). The lightweight AlTiVCr CCA shows a domain-like structure as displayed in the dark field (DF) transmission electron microscopy (TEM) micrograph (Fig. 2a), which was taken using the circled (100) superlattice reflection from the selected area electron diffraction (SAED) pattern (the insert in Fig. 2a).

In terms of $Al_{0.9}FeCrCoNi$ alloy, the grain boundary phase is of an FCC structure, the modulated microstructure is determined to be nano-scale interconnected BCC and B2 phase. As previously described[23], the FCC phase is Co–Fe–Cr rich, BCC phase is Fe–Cr rich while B2 phase is Ni–Al rich. These two CCAs exhibit outstanding room-temperature properties including high

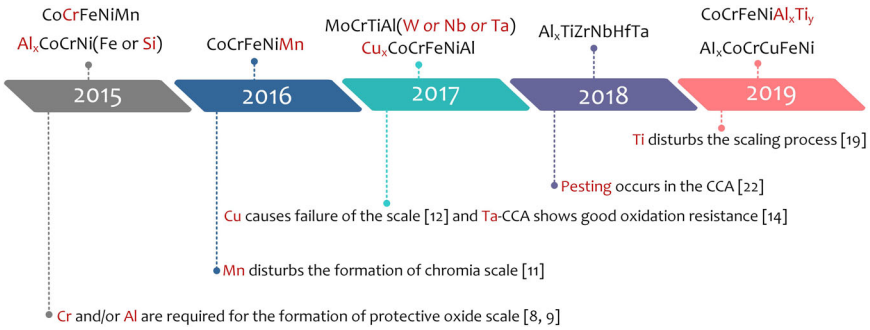

Fig. 1 Research on oxidation of HEAs (and CCAs). A compact summary of the studies on high-temperature oxidation performance of CCAs in the period 2015 todate (Details are presented in Table 1).

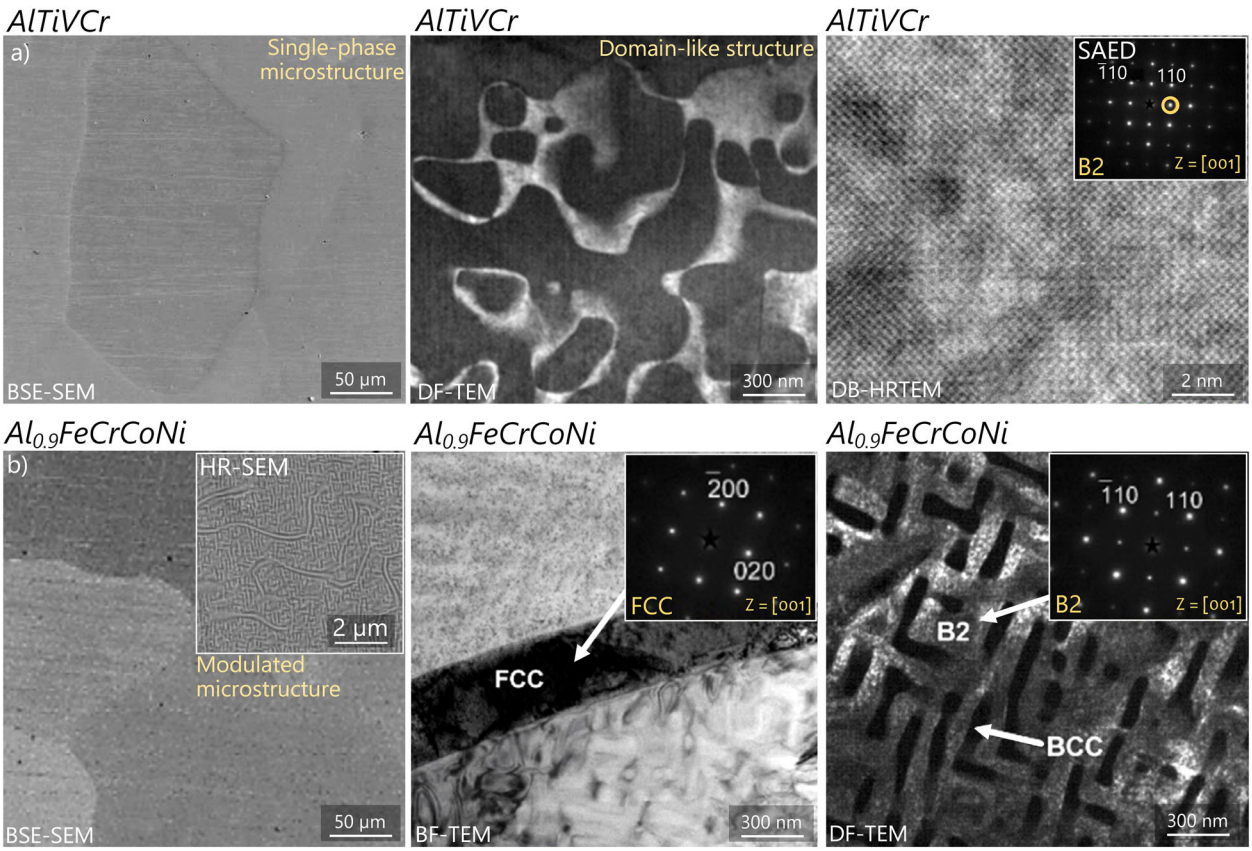

Fig. 2 SEM and TEM (Dark field, bright field, and high-angle annular dark field imaging, as well as selected area electron diffraction) analysis revealing the microstructure of. a the AlTiVCr CCA, and **b** the $Al_{0.9}FeCrCoNi$ CCA. The microstructure of the alloys is further described in[7,23,24].

hardness and superior aqueous corrosion resistance as compared with e.g., 304SS[7,23,24]. Herein, the high-temperature oxidation performance of the two CCAs was studied for the first time at 700 and 900 °C.

TGA experiments

The mass change of the alloys under investigation as a function of time, as well as microscopy results revealing the surface morphology and chemistry of the two CCAs after oxidation experiments at 700 and 900 °C are presented in Fig. 3.

For comparison, mass change values as a function of time for three other CCAs (from the literature) are also included in Fig. 3a. Following 24 h oxidation at 700 °C, AlTiVCr and $Al_{0.9}FeCrCoNi$ had a specific mass gain ($X = \Delta m/A$) of ~3 and 0.12 mg/cm^2, respectively. At 900 °C, AlTiVCr and $Al_{0.9}FeCrCoNi$ showed a specific mass gain of ~17.4 and 0.55 mg/cm^2, respectively. Comparing these values with specific mass gains reported for other CCAs (see e.g., Fig. 3a) and for Ni-base or Fe-base high-temperature alloys and superalloys (<0.5 mg/cm^2)[25,26], it becomes apparent that the mass gain values of $Al_{0.9}FeCrCoNi$ CCA are low, suggesting that the $Al_{0.9}FeCrCoNi$ CCA is oxidation resistant in the studied environment at 700 and 900 °C (in terms of mass gain).

A careful assessment of the mass gain data revealed that both alloys obey the parabolic rate law ($X^2 = k_p t$), after a short initial period of transient oxidation, i.e. the linear rate law ($X = k_c t$). According to the well-established Wagner's theory[27], an oxidation process would follow a parabolic rate law, if the growth of scale is diffusion controlled. Wagner described the formation of oxide

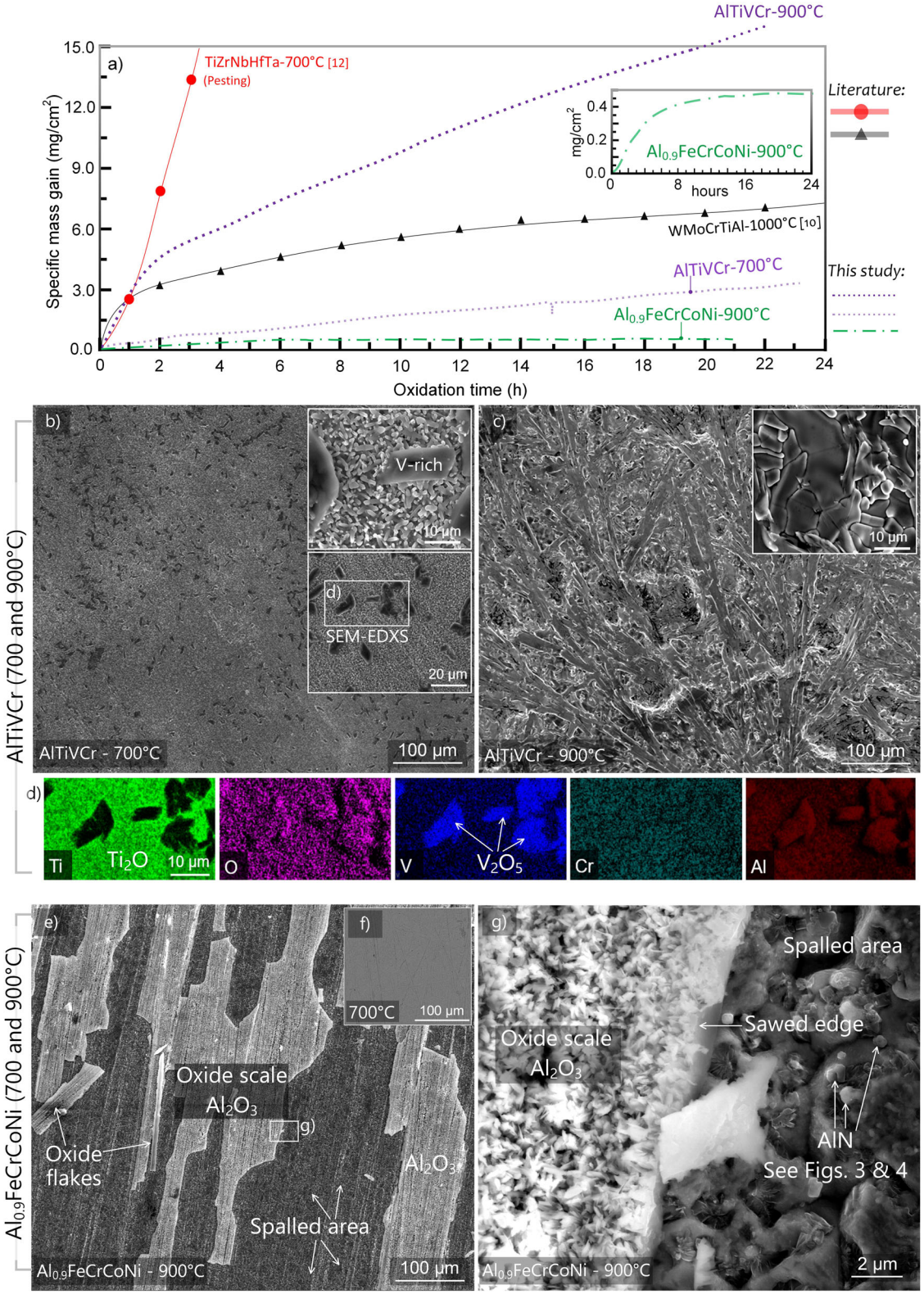

Fig. 3 Oxidation and microscopy analysis. a Specific mass-gain curves of the CCAs under investigation and three CCAs from the literature (provided for the sake of comparison), **b**–**d** SEM-energy-dispersive X-ray spectroscopy (EDXS) analysis revealing the surface morphology and oxides of the AlTiVCr CCA after exposure at 700 and 900 °C for 24 h, and **e**–**g** SEM-EDXS analysis of the $Al_{0.9}FeCrCoNi$ CCA after exposure at 700 and 900 °C for 24 h. Note (1): The phases designated in the SEM micrographs were identified using EDXS and X-ray diffraction (XRD). Note (2) some irregularities such as small weight losses were observed in the mass gain curves which could be due to scale spallation.

scale as an electrochemical process with a cathode at the scale/gas surface and an anode at the alloy/scale interface[1,2,27–29]. Therefore, it is reasonable to suggest that the alloys are capable of forming of a protective oxide scale on their surfaces during oxidation at 700 and 900 °C.

Post-exposure analysis

The oxidation morphology of the CCAs was studied by microscopy (Figs 3–5). At both temperatures, the surface of AlTiVCr was fully covered by Ti-rich and V-rich oxides (Fig. 3b–d), whereas Al_2O_3 was found on the surface of $Al_{0.9}$FeCrCoNi (Fig. 3e–g). Despite the low mass gain (Fig. 3a) and the evidence for the formation of Al_2O_3 on the surface of $Al_{0.9}$FeCrCoNi, the Al_2O_3 layer tended to spall from the substrate (Fig. 3e). Therefore, the corresponding oxidation features, including oxide flakes, sawed edges and ″bare″ alloy surface (designated as spalled area in Figs 3g and 4) were observed in the plan-view SEM micrographs.

A better understanding of the mechanisms by which barrier (oxide) layer fails is crucial for enabling the development of CCAs with improved ability to withstand high-temperature corrosion. Indeed, the phenomenon observed in the SEM images is significant to understand as the adhesion and spallation behaviour of an oxide scale defines its protective characteristics during an oxidation exposure. It is suggested that the observed spallation (Fig. 3g) could be ascribed to high thermal stresses developed within the substrate and the oxide layer during the cooling part of the exposure. This, in turn, could be due to the molar volume alterations produced by oxidation of CCAs, as well as a large difference in coefficients of thermal expansion (CTEs) of the CCA substrate and Al_2O_3. While there are limited studies on thermophysical properties of CCAs, it has been reported that, at ~800 °C, the CTE of Al_xFeCrCoNi system could reach 27×10^{-6} K^{-1} [26]. This value is significantly higher than Al_2O_3, which tends to remain $<11.5 \times 10^{-6}$ K^{-1} at a range of temperatures (and note that CTE of the advanced high-temperature alloy Kanthal APMT^{TM} at 20–1000 °C is 14.7×10^{-6} K^{-1})[1,2].

Chemical composition analysis revealed the formation of sub-micron sized AlN particles embedded into the substrate at the interface between the alloy surface and the Al_2O_3 layer (Figs 4 and 5). When the oxide scale fails to protect the alloy, molecular nitrogen dissolves in the alloy. The nitrogen molecules become dissociated at the alloy/oxide interface and absorption of nitrogen atoms occurs by the substrate. Note that nitridation is also known to reduce the Al activity within alloy and could cause embrittlement of the spallation of the scale[1,2], in agreement with the observations in the case of the $Al_{0.9}$FeCrCoNi CCA.

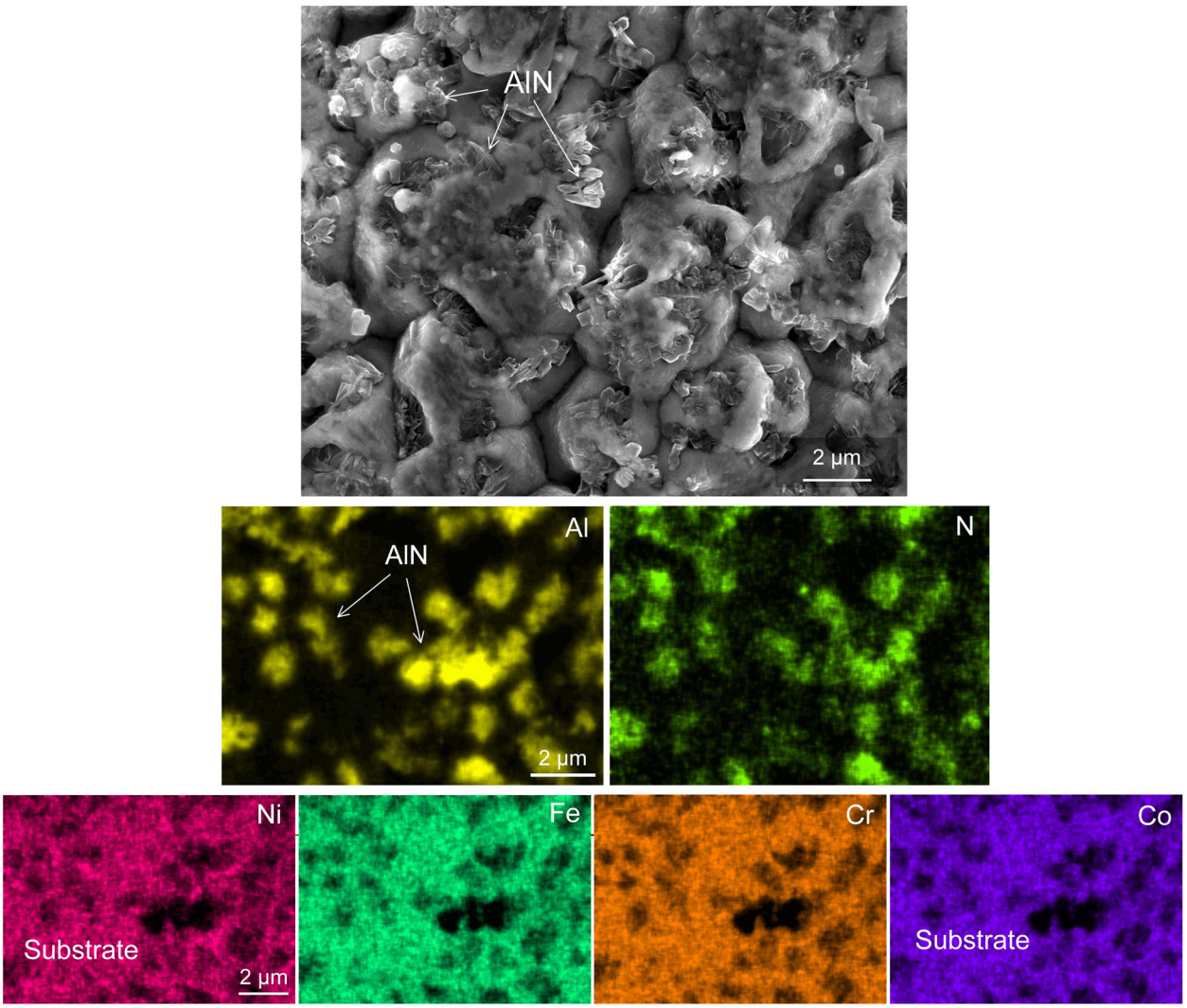

Fig. 4 SEM-EDXS analysis revealing the surface morphology of the $Al_{0.9}$FeCrCoNi CCA after exposure at 900 °C for 24 h. Note the formation of AlN particles in the spalled areas.

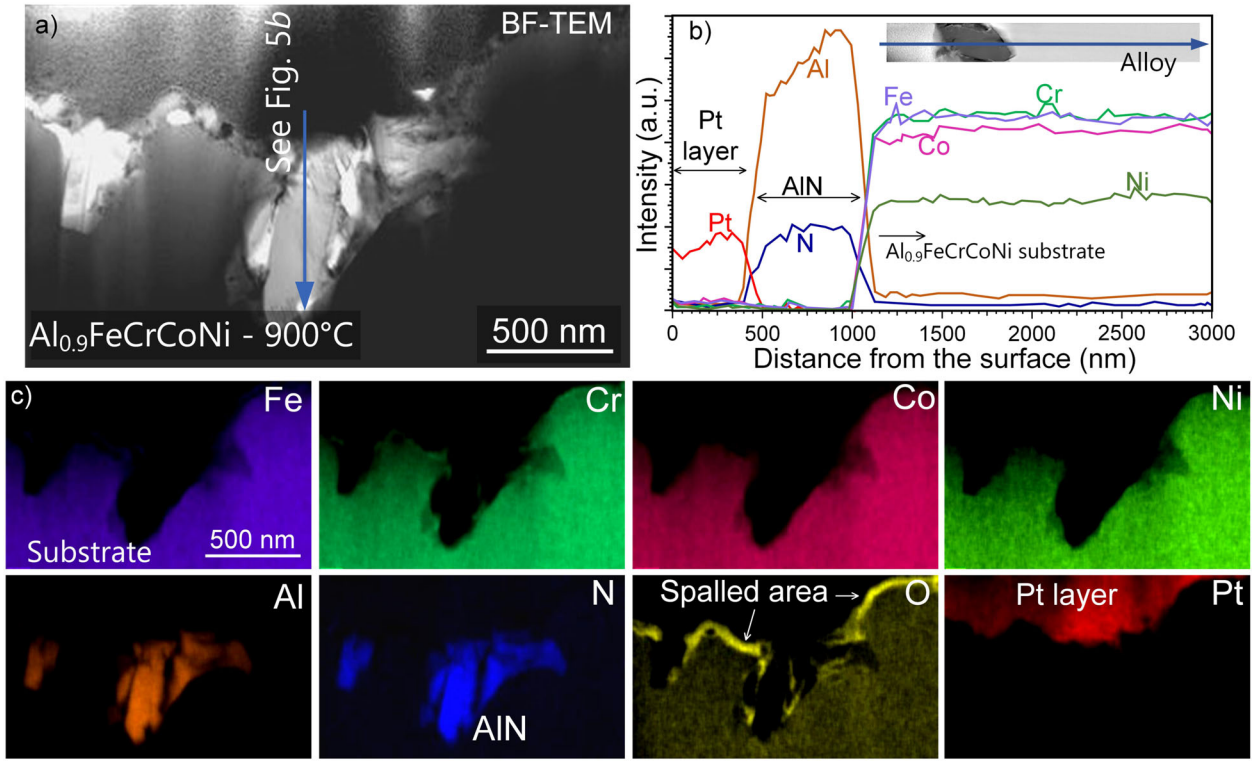

Fig. 5 STEM-EDXS analysis on the cross-section of the $Al_{0.9}FeCrCoNi$ CCA after exposure at 900 °C for 24 h. Note that the FIB-prepared thin foil revealing internal nitridation in the CCA was extracted from the spalled area viewed in Figs 3g and 4.

The formation of oxidation products formed on the CCAs was investigated using XRD, microscopy and equilibrium calculations (Figs 6 and 7). While XRD and electron microscopy analysis are two well-established methods that are commonly used to study the microstructure and structure of oxidation products, to the best of our knowledge, the Calculation of Phase Diagrams (CALPHAD) approach has not been used to study the oxidation of CCAs. However, it is noted that this approach has been used for more than three decades in the field of materials design[30]. In the CALPHAD method, thermodynamic properties of the system predict stable phases under different conditions e.g., temperature, pressure, and composition. Thermodynamic properties are modelled by phenomenological models based on atomistic simulations and experimental data and stored in the databases built by using a CALPHAD-based software. Such databases are the main input to explain and predict materials microstructure and possible products in different circumstances. The TCHEA3 database for CCAs has previously used to study the phases formed in the bulk material of several CCAs[31]. In the present case, the SSUB6 database for compounds was combined with the TAHEA3 to predict different phases that may form at temperatures of interests when the partial pressure of oxygen varies.

From the XRD patterns, it could be suggested that a wide range of oxides (TiO_2 (rutile), Al_2O_3, $TiVO_4$, and V_2O_5) were the principal oxidation products on the AlTiVCr after oxidation at 700 and 900 °C (see e.g., Fig. 6a). It is, however, cautioned that it was challenging to distinguish some of the peaks/phases due to their similar characteristics and a large number of high-to-low intensity peaks could not be assigned to any known phases. In the case of the $Al_{0.9}FeCrCoNi$ CCA oxidised at 900 °C, the XRD pattern displayed peaks that could be assigned to Al_2O_3, with the corundum structure, and AlN. The peaks showing the characteristics of FCC, BCC, and B2 phases were sourced by the substrate and XRD disclosed the formation of the Sigma phase in the $Al_{0.9}FeCrCoNi$ CCA both at 700 and 900 °C, which is an expected observation[32].

Given that a key factor governing oxidation behaviour is the integrity of the oxide layer in terms of porosity, cracking, and adhesion to the alloy substrate, cross-sectional analysis (Fig. 6c) was also carried out. Following oxidation at 900 °C, the AlTiVCr CCA formed an defect-free (i.e., dense), thick (95 ± 25 µm) and multi-layered oxide scale consisting of V_2O_5 (as the uppermost layer), following by V and Cr-containing TiO_2, $(Al,Cr)_2O_3$ and an inner layer of $TiO_2 + Al_2O_3$ (Fig. 6c). The presence of all alloying elements in the thick oxide layer forming on the surface of this alloy indicates that the AlTiVCr CCA was unable to establish a protective oxide scale during exposure, which agrees well with the mass gain data (Fig. 3a).

The observation that Cr and V are soluted in the TiO_2 structure —$Ti_{1-x-y}V_xCr_yO_2$, with Cr + V filling <5 at. % of the oxide structure —agrees with the findings of a previous study on oxidation of some selective AlTiVCr-containing refractory CCAs[33]. Of the detected oxides, V_2O_5 is considered as an "unwelcome" reaction product and thus its formation should be suppressed because its low melting point (~690 °C) and boiling point (1750 °C) makes it susceptible to volatile or fuse at the temperature foreseen[34]. While SEM investigations (Fig. 3b–d) showed no surface feature that could be ascribed to the formation of molten V_2O_5 during the oxidation exposures at 700 and 900 °C, a yellow matter was noted on the interior surface of the crucibles after the oxidation experiment of the AlTiVCr CCA. Note that the observed yellowish matter inside the crucible was identical to the feature that has previously been reported and attributed to the formation of molten V_2O_5, e.g., in the case of Ti-6Al-4V exposed to oxidising environments at elevated temperatures[35].

Indeed, the formation of V-doped TiO_2 is not surprising bearing in mind the ionic radius of V^{4+} (0.72 Å), which is close to that of Ti^{4+} (0.74 Å). As such, V^{4+} can incorporate into the TiO_2 crystal lattice and effectively substitutes for Ti^{4+} forming a $Ti_{1-x}V_xO_2$ solid-solution phase[36]. At 700 °C, a somewhat similar, but thinner (8 ±

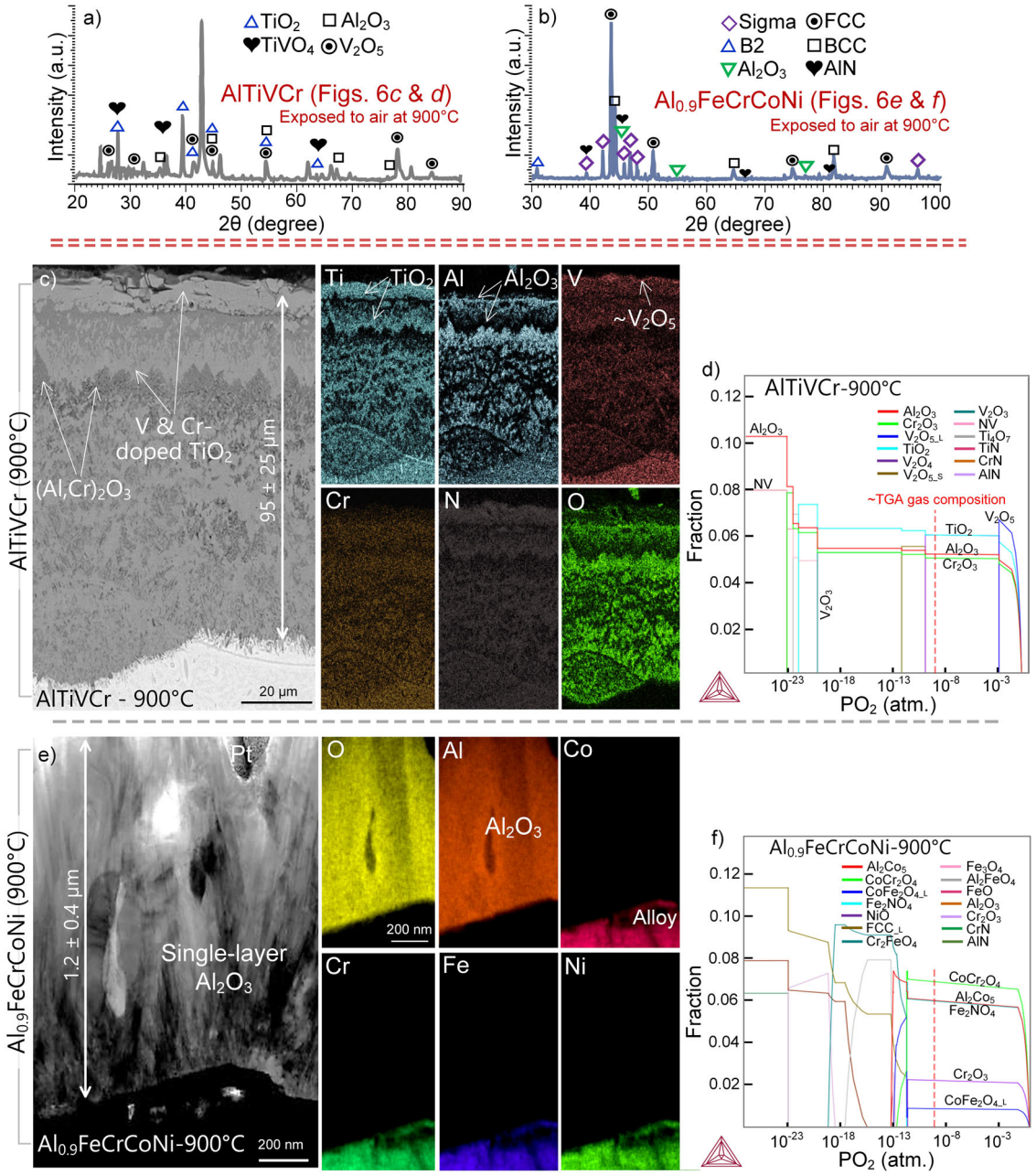

Fig. 6 Oxidation products and the surface films. a and **b** XRD patterns from the CCAs after the oxidation exposure at 900 °C, **c**, **e** SEM-STEM-EDXS analysis of the CCAs after exposure at 900 °C, **d** and **f** variation of phase fractions versus partial pressure of oxygen for the two CCAs at 900 °C. Note (1): The partial pressure corresponding to experimental condition herein (~10^{-9} atm) is marked by a dashed red line. Note (2): There are overlapping X-ray peaks from N and Ti (see the co-occurrence in the N and Ti EDXS maps in Fig. 6c).

2.4 µm), layered oxide scale was found on the surface of the AlTiVCr CCA (Fig. 7). Finally, it should be noted that there was a reasonable agreement between the experimental (XRD/SEM-EDXS) data and the results obtained from equilibrium calculations in the case of the AlTiVCr (Fig. 6a, c versus Fig. 6d).

In regards to the $Al_{0.9}FeCrCoNi$ CCA, as was expected from the mass gain data (Fig. 3a), the alloy showed a thin (1.2 ± 0.4 µm) single-layered Al_2O_3 (compare Fig. 6c, e), which is highly desirable in the context of oxidation resistance. It should, however, be noted that in the case of the $Al_{0.9}CrCoNiFe$ CCA, while experimental results showed Al_2O_3 and AlN as the oxidation products, equilibrium calculations using Thermo-Calc predicted the formation of various mixed oxides and spinels such as $CoCr_2O_4$, $CoFe_2O_4$, as well as chromia (Cr_2O_3), which remains an open issue for a future study.

DISCUSSION

The long-term durability of the protective oxide scales relies on the ability of the scale to maintain its integrity over time. The results presented herein, along with findings in the literature to date, indicate that CCAs, whilst thermally stable, are yet to designed for the demanding applications, where high-temperature corrosion and oxidation is an issue. As an example, in the case of the AlTiVCr CCA, it is suggested that an increased

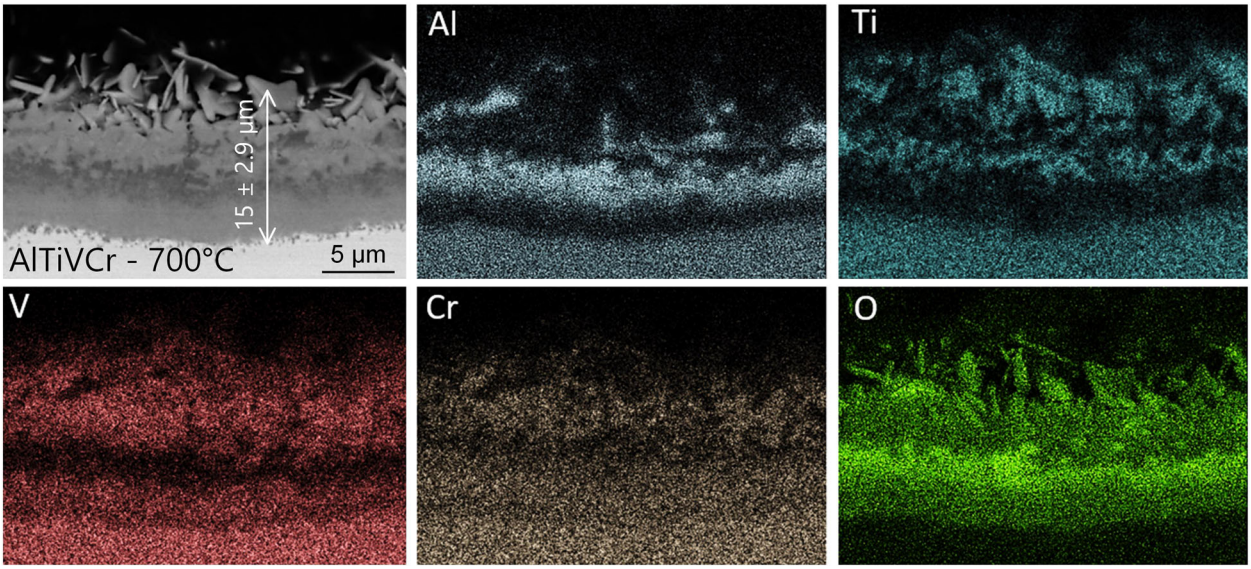

Fig. 7 SEM-EDXS analysis on the cross-section of the AlTiVCr CCA after exposure at 700 °C for 24 h. The cross-sectional analysis presented here may be compared with Fig. 6c.

concentration of Al (e.g., Al_2TiVCr) is required for the alloy to suppress the formation of the fast-growing Ti-containing and V-containing oxides and to ensure the formation of a protective Al_2O_3 scale. Furthermore, a future design strategy could be trace addition (~0.1 at. %) of the so-called reactive elements such as Y, Hf, Zr, and Ce into the CCAs. These elements are well-known to improve the high-temperature oxidation performance of current state-of-the-art Fe-base and Ni-base alloys by orders of magnitude through enhancing the plasticity and adherence of the scale (comprising Cr_2O_3 and/or Al_2O_3). Thus, future studies on alloys with such compositional alterations which target the high-temperature oxidation properties would be rewarding.

The disagreement between thermodynamic calculations results and the experimental observations can be due to one of the following reasons: (i) the thermodynamic calculations are for the equilibrium state and there is a possibility that equilibrium is not reached in the samples, (ii) although some of the reactions predicted by the equilibrium calculations are thermodynamically favoured, the kinetics of some of the other reactions may be stronger and has taken over the path of the system, and (iii) there has not been any experimental study for this system and the databases are based on extrapolations from similar systems. Thus, it is suggested that the databases can be re-assessed based on the new findings. These results show the necessity for further investigations of these systems to provide required input for the CALPHAD assessments for oxidation of CCAs.

In summary, the following conclusions were derived from this study:

The oxidation exposures performed over a period of 24 h resulted in specific mass gains of 3 (at 700 °C) and 17.4 mg/cm^2 (at 900 °C) in the AlTiVCr CCA. The corresponding values for the $Al_{0.9}$FeCrCoNi CCA were considerably lower (0.12 and 0.55 mg/cm^2). The two alloys followed the parabolic rate law. Thus, the oxidation process in the CCAs can be described by the classical Wagnerian-type theory. It was also noted that the AlTiVCr CCA reached the steady-state oxidation after a slightly longer time than the $Al_{0.9}$FeCrCoNi CCA.

Post-exposure analysis using XRD and electron microscopy revealed that while TiO_2 (in the form of $Ti_{1-x-y}V_xCr_yO_2$ showing the structure of rutile), Al_2O_3 and V_2O_5 were the oxidation products of AlTiVCr in the studied condition, the $Al_{0.9}$FeCrCoNi CCA formed a single-layered Al_2O_3 scale with minor fraction of AlN particles at the alloy/oxide scale interface. Future studies are needed to explain the mechanism by which (internal) nitridation occurred in the latter CCA.

The scale forming on AlTiVCr was adherent to the alloy surface, whereas some degree of spallation was observed in Al_2O_3 scale formed on the $Al_{0.9}$FeCrCoNi CCA. It was suggested that a relatively large mismatch with the thermal expansion coefficient of alumina and the underlying alloy was the main reason for the rather extensive spallation observed herein.

The CALPHAD approach was employed to predict the oxidation products of the CCA and it provided useful guidelines for understanding the oxidation process in the case of the AlTiVCr CCA. However, no agreement was found between the experimental results and thermodynamic calculations in the case of the $Al_{0.9}$FeCrCoNi CCA, which was discussed in terms of equilibrium conditions and the limitations of the current thermodynamic databases. It is suggested that findings from this work be utilised to further inform thermodynamic databases for CCAs.

METHODS

Sample preparation

The AlTiVCr and $Al_{0.9}$FeCrCoNi studied herein were produce by arc melting in an argon atmosphere. The lightweight AlTiVCr CCA had an equi-atomic composition of 15.1Al, 26.9Ti, 28.6 V, 29.2Cr (in wt.%) and the $Al_{0.9}$FeCrCoNi CCA had a chemical composition of 3.4Al, 25.2Co, 22.2Cr, 23.9Fe, 25.1Ni (in wt.%)[7,23]. Both CCAs were melted on a water-cooled copper hearth, with pure (99.9 wt.%) metal chunks as the starting materials. The ingots were remelted five times to improve the homogeneity. The material was machined to produce 15 × 15 × 3 mm^3 test coupons for the oxidation experiments. The coupons were then ground using silicon carbide abrasive paper (to P4000 grit).

Oxidation experiments

Oxidation experiments were performed using a simultaneous thermogravimetric analyser (TGA, NETZSCH STA 449F3 Jupiter) in a Pt-furnace and dense alumina crucibles. The total flow rate of the gases was kept constant at 50 ml/min; 10 ml/min N_2 and bal. laboratory air during the isothermal period, and pure N_2 during the ramp up/down. For each experiment, the heating and cooling ramp rates of 40 K/min and an isothermal period of 22 h was used. A baseline correction using empty crucibles and same experimental conditions was performed to minimise the effect of gas

switching during cycling. The Proteus software from NETZSCH was used to analyse and evaluate the corrected weight change.

Characterisation of oxidation and microstructure

Following the TGA experiments, the cross-section of the CCAs were mounted, ground and polished using the procedure described in[37,38]. Shortly, the cross-section of the CCAs were mounted, ground and polished using diamond suspensions towards a 1 µm and then 0.25 µm mirror-like finish on a Buehler Microcloth® for 15–35 min. The preparation procedure was included cleaning in ethanol, agitation and rinsing in ethanol, and storing the specimens in over a desiccant. The phase structure of CCAs and oxidation products (including oxides and nitrides) were analysed using a Bruker D8 Advance X-ray diffractometer with Cu-Kα radiation ($\lambda = 0.154$ nm) functioning at 40 kV and 40 mA. The XRD data were then evaluated by means of ICDD PDF 4 and Bruker Eva® software. Microstructural and surface morphology of specimens were examined using FEI Quanta 3D-FEG and FEI Nova NanoSEM 450 scanning electron microscopes (SEM), both equipped with energy dispersive X-ray spectroscopy (EDXS) from Oxford instruments AZtec® X-ray analysis system. The SEM was operated at 10–20 kV during imaging (using the backscattered electron (BSE) and secondary electron (SE) modes) and at 10–15 kV during the EDXS analysis (for line-scan, point analysis, as well as elemental mapping).

In addition, the oxide scale formed was also investigated at higher resolutions by means of scanning transmission electron microscopy (STEM) imaging and EDXS analysis using an FEI Tecnai G2 T20 operating at an accelerating voltage 200 kV and equipped with a Bruker XFlash 6TI30 X-ray detector. TEM micrographs were captured using the bright field (BF), dark field (DF) and high-angle annular dark-field (HAADF) modes. Specimens for TEM were fabricated by means of focused ion beam (FIB) FEI Quanta 3D-FEG. Thin foils were milled from the oxidised CCAs by means of Ga ion milling, followed by lift out onto a Cu grid, and a final stage of by a thinning process of the foil to ~100 nm in thickness.

Equilibrium calculations

Thermodynamics calculations were performed using Thermo-Calc software (Thermo-Calc Software AB, Stockholm, Sweden)[39] in order to test the potential of using existing databases for oxidation in CCAs. Thermo-Calc is a Calculation of Phase Diagrams (CALPHAD)-based software that can predict phases that form in different conditions. It should be noted that the calculations presented herein originate from the ordinary oxide database in combination with CCAs database since there is no explicit database for oxide phases in CCAs in none of the CALPHAD software. The agreement between calculations and experimental results can determine the accuracy of these databases for the present application.

DATA AVAILABILITY

The data that support the findings of this study are available from the corresponding authors upon reasonable request.

Received: 20 January 2020; Accepted: 15 July 2020;
Published online: 13 August 2020

REFERENCES

1. Mortazavi, N. et al. Interplay of water and reactive elements in oxidation of alumina-forming alloys. *Nat. Mater.* **17**, 610–617 (2018).
2. Kofstad, P. *High Temperature Corrosion*. (Elsevier, London/New York, 1988).
3. Chyrkin, A. et al. Effect of thermal cycling on protective properties of alumina scale grown on thin Haynes 214 foil. *Corros. Sci.* **98**, 688–698 (2015).
4. Weiser, M. et al. Transport mechanisms during the high-temperature oxidation of ternary γ/γ′ Co-base model alloys. *NPJ Mater. Degrad.* **3**, 33 (2019).
5. Moussa, S. O. & Morsi, K. High-temperature oxidation of reactively processed nickel aluminide intermetallics. *J. Alloy. Compd.* **426**, 136–143 (2006).
6. Chen, J. et al. A review on fundamental of high entropy alloys with promising high–temperature properties. *J. Alloy. Compd.* **760**, 15–30 (2018).
7. Qiu, Y. et al. A lightweight single-phase AlTiVCr compositionally complex alloy. *Acta Mater.* **123**, 115–124 (2017).
8. Butler, T. M., Alfano, J. P., Martens, R. L. & Weaver, M. L. High-temperature oxidation behavior of Al-Co-Cr-Ni-(Fe or Si) multicomponent high-entropy alloys. *JOM* **16**, 246–259 (2015).
9. Holcomb, G. R., Tylczak, J. & Carney, C. Oxidation of CoCrFeMnNi high entropy alloys. *JOM* **67**, 2326–2339 (2015).
10. Kai, W. et al. The oxidation behavior of an equimolar FeCoNiCrMn high-entropy alloy at 950 °C in various oxygen-containing atmospheres. *Corros. Sci.* **108**, 209–214 (2016).
11. Laplanche, G., Volkert, U. F., Eggeler, G. & George, E. P. Oxidation behavior of the CrMnFeCoNi high-entropy alloy. *Oxid. Met.* **85**, 629–645 (2016).
12. Dabrowa, J. et al. Influence of Cu content on high temperature oxidation behavior of AlCoCrCuxFeNi high entropy alloys (x = 0; 0.5; 1). *Intermetallics* **84**, 52–61 (2017).
13. Kai, W. et al. Air-oxidation of FeCoNiCr-based quinary high-entropy alloys at 700–900 °C. *Corros. Sci.* **121**, 116–125 (2017).
14. Gorr, B. et al. High-temperature oxidation behavior of refractory high-entropy alloys: effect of alloy composition. *Oxid. Met.* **88**, 339–349 (2017).
15. Müller, F. et al. Effect of microalloying with silicon on high temperature oxidation resistance of novel refractory high-entropy alloy Ta-Mo-Cr-Ti-Al. *Mater. High. Temp.* **35**, 168–176 (2018).
16. Kim, Y., Joo, Y., Kim, H. S. & Lee, K. High temperature oxidation behavior of Cr-Mn-Fe-Co-Ni high entropy alloy. *Intermetallics* **98**, 45–53 (2018).
17. Chen, L. et al. High temperature oxidation behavior of Al0.6CrFeCoNi and Al0.6CrFeCoNiSi0.3 high entropy alloys. *J. Alloy. Compd.* **764**, 845–852 (2018).
18. Liu, C. M., Wang, H. M., Tang, H. B. & Zhang, A. L. Microstructure and oxidation behavior of new refractory high entropy alloys. *J. Alloy. Compd.* **583**, 162–169 (2014).
19. Erdogan, A., Doleker, K. M. & Zeytin, S. Effect of Al and Ti on high-temperature oxidation behavior of CoCrFeNi-based high-entropy alloys. *JOM* **71**, 3499–3510 (2019).
20. Kai, W. et al. The corrosion of an equimolar FeCoNiCrMn high-entropy alloy in various CO_2/CO mixed gases at 700 and 950 °C. *Corros. Sci.* **153**, 150–161 (2019).
21. Liu, Y. et al. Effect of Al content on high temperature oxidation resistance of AlxCoCrCuFeNi high entropy alloys (x = 0, 0.5, 1, 1.5, 2). *Vaccum* **169**, 108837 (2019).
22. Chang, C., Titus, M. S. & Yeh, J. Oxidation behavior between 700 and 1300 °C of refractory TiZrNbHfTa high-entropy alloys containing aluminum. *Adv. Eng. Mater.* **20**, 1700948 (2018).
23. Sato, A., Chiu, Y.-L. & Reed, R. Oxidation of nickel-based single-crystal superalloys for industrial gas turbine applications. *Acta Mater.* **59**, 225–240 (2011).
24. Wagner, C. The theory of the warm-up process. *Z. Phys. Chem.* **21B**, 25–41 (1933).
25. Hellström, K. et al. Oxidation of a dispersion-strengthened powder metallurgical FeCrAl alloy in the presence of O2 at 1,100 °C: the influence of water vapour. *Oxid. Met.* **83**, 533–558 (2015).
26. Chou, H. P., Chang, Y. S., Chen, S. K. & Yeh, J. W. Microstructure, thermophysical and electrical properties in AlxCoCrFeNi (0 ≤ x≤ 2) high entropy alloys. *Mater. Sci. Eng. B* **163**, 184–189 (2009).
27. Zhang, C. et al. Understanding phase stability of Al–Co–Cr–Fe–Ni high entropy alloys. *Mater. Des.* **109**, 425–433 (2016).
28. Du, H. L., Datta, P. K., Lewis, D. B. & Burnell-Gray, J. S. Air oxidation behaviour of Ti-6AL-4V alloy between 650 and 850 °C. *Corros. Sci.* **36**, 631–642 (1994).
29. Dean, J. A. (ed.) *Lange's Handbook of Chemistry*. (McGraw-Hill, New York, 1998).
30. Guangbao, M., Kai, Y., Pengfei, B., Congqian, C. & Xiaohua, M. High temperature oxidation and wear behaviors of Ti–V–Cr fireproof titanium alloy. *Metals* **7**, 226 (2017).
31. Klosek, S. & Raftery, D. Visible light driven V-doped TiO_2 photocatalyst and its photooxidation of ethanol. *J. Phys. Chem. B* **105**, 2815–2819 (2001).
32. Mortazavi, N. et al. In situ ESEM investigation of KCl-induced corrosion of a FeCrAl and a model FeNiCrAl alloy in lab air at 450 °C. *J. Electrochem. Soc.* **162**, C744–C753 (2015).
33. Andersson, J. O., Helander, T., Höglund, L., Shi, P. & Sundman, B. Thermo-Calc & DICTRA, computational tools for materials science. *Calphad* **26**, 273–312 (2002).
34. Esmaily, M. et al. Corrosion behavior of alloy AM50 in semisolid cast and high-pressure die cast states in cyclic conditions. *Corosion* **71**, 737–748 (2015).
35. Kaufman, L. & Ågren, J. CALPHAD, first and second generation–Birth of the materials genome. *Scr. Mater.* **70**, 3–6 (2014).
36. Sanchez, J. M. et al. Phase prediction, microstructure and high hardness of novel light-weight high entropy alloys. *J. Mater. Res. Technol.* **8**, 795–803 (2019).
37. Qiu, Y. et al. Microstructural evolution, electrochemical and corrosion properties of AlxCoCrFeNiTiy high entropy alloys. *Mater. Des.* **170**, 107698 (2019).
38. Qiu, Y., Thomas, S., Gibson, M. A., Fraser, H. L. & Birbilis, N. Corrosion of high entropy alloys. *NPJ Mater. Degrad.* **1**, 15 (2017).
39. Naumenko, D., Quadakkers, W. J., Galerie, A., Wouters, Y. & Jourdain, S. Parameters affecting transient oxide formation on fecral based foil and fibre materials. *Mater. High. Temp.* **20**, 287–293 (2003).

ACKNOWLEDGEMENTS

M.E. thanks the Swedish Research Council, The Royal Swedish Academy of Engineering Sciences and Helge AX:son Johnsons Stiftelse for the financial support. The authors acknowledge use of facilities within the Monash Centre for Electron Microscopy (MCEM) and The Monash X-ray Platform (MXP).

AUTHOR CONTRIBUTIONS

M.E., Y.Q., and M.B.V., carried out the experimental studies, which included the oxidation experiments, electron microscopy (SEM-EDX, FIB, TEM, and STEM-EDX), as well as XRD analysis. S.B. conducted the equilibrium calculations using the CALPHAD approach. All authors contributed in drafting or revising the paper. A.A. and N.B. supervised the study.

COMPETING INTERESTS

The authors declare no competing interests.

ADDITIONAL INFORMATION

Correspondence and requests for materials should be addressed to M.E.

Reprints and permission information is available at http://www.nature.com/reprints

Publisher's note Springer Nature remains neutral with regard to jurisdictional claims in published maps and institutional affiliations.